# Asymmetry of hydrogen lines in plasmas utilizing a statistical description of ion-quadrupole interaction in Mozer-Baranger limit

**J. Halenka**

Institute of Physics, Pedagogical University, Oleska 48, PL-45-052 Opole, Poland

Received 1 August 1989; final version 30 January 1990

Hydrogen line Stark profiles are calculated in the static ion approximation including the ion-quadrupole interaction and the quadratic Stark effect. The statistics of the ion-quadrupole interaction is evaluated in the Mozer-Baranger limit taking into account the screening and the ion correlations. The generalized function $B_\rho(\beta)$ exceeds several times the ordinary Chandrasekhar and von Neumann function $B(\beta)=B_{\rho=0}(\beta)$ (i.e. $B_\rho(\beta)$ at $\rho=0$) and in the same proportion increases the importance of the ion-quadrupole interaction. For $n_e$ ranging from $10^{16}$ to $10^{18}\,\mathrm{cm}^{-3}$, calculated parameters of the asymmetry and shift of $H_\beta$ agree well with measurements by different authors.

**PACS:** 32.60.S; 32.70

## 1. Introduction

In the approximation of plasma-emitter dipole interaction, the profiles of hydrogen (and H-like ions) lines calculated in the first order of perturbation theory are symmetric and unshifted, independent of assumptions concerning the ion motion (static, e.g. [1], and dynamic, e.g. [2], ions). To explain the observed shifts and asymmetries of H-line profiles, corrections with respect to this description [1] of the emitter-plasma interaction are introduced and the second order of perturbation theory (quadratic Stark effect) is included into the dynamic approximation for electrons and the static one for ions [3–9].

The main cause of the red shifts of H-lines is the interaction of the emitter with free electrons, whereas the asymmetry results mainly from inhomogeneities of the ionic field and, to a smaller extent, from the static quadratic Stark effect. Fine structure splitting is an additional source of asymmetry [10], which in the case of line profiles of H-line Ne $X$ is of opposite sign and of the same order of magnitude as the asymmetry resulting from emitter-ion-quadrupole interaction (EIQI) and the static quadratic Stark effect. However, due to its very strong dependence on the radiator nuclear charge, this source of asymmetry is negligibly small for H-atoms.

The specific shape of the profile of the hydrogen Balmer line $H_\beta$ allows to define separate parameters of shift and asymmetry, and to isolate the contributions of electrons to the shift and of ions to the asymmetry [9, 11, 12]. It was shown [9, 12] that the asymmetry of $H_\beta$ measured in a wide range of the electron densities $n_e$ nearly twofold exceeds the asymmetry calculated taking into account the EIQI, the static quadratic Stark effect, and the so-called trivial asymmetry. In this calculations, EIQI have been taken alternatively, i.e. as in [5] or [7]. As suggested in [9, 12], such great discrepancy between calculations and measurements evidences unsatisfactory description of EIQI.

Kudrin and Sholin [5] were first to show that the inhomogeneities of ion-produced field can cause the asymmetry of the $H_\beta$ peaks. In [5, 6] EIQI was described in the Nearest Neighbour Limit. This approach was generalized by Demura and Sholin [7] by introducing the joint probability distribution function for the electric microfield strength and the microfield gradients in Holtsmark Limit (i.e., taking into account all the uncorrelated and unscreened ions). In this approximation the mean field gradients are proportional to the Chandrasekhar and von Neumann [13] function $B(\beta)$. Joyce et al. [10] included the EIQI to the description of the profiles of lines emitted by highly ionized H-like ions in the Independent Perturber Model (screened but uncorrelated ions) [14]. Lewis and Margenau [15] have used this model to calculate the high-frequency (electronic) component of the microfield distribution. This model corresponds to that which has been proposed by Ecker and Müller [16] for low-frequency (ionic) component of the microfield distribution.

The aim of this paper is to include the ion-quadrupole-interaction into the description of the H-line profile, using the statistical description of microfield gradients in the Mozer-Baranger Limit (i.e., taking into account the screening effect and the ion correlations), and to rean-

alyze the asymmetry and shift of $H_\beta$. We realize that the microfield distribution calculated by the technique proposed by Hooper [17] i.e. taking into account all the correlations, is more accurate than that obtained in the $M-B$ Limit, where only pair correlations are taken into account. However, the differences between the microfield distributions obtained in these two ways are rather small and therefore we assume that it is sufficient to calculate the microfield gradients distribution exact to the pair correlations.

## 2. Ion-quadrupole interaction

In the static ion approximation, the Hamiltonian of a H-atom in a plasma, including inhomogeneities of the ionic field and the shielding of ions by free electrons, is

$$H = H_0 - \mathbf{d}\cdot\mathbf{E} - 1/6\sum_{ij} Q_{ij}E_{ij} + 1/6\, e_0 r^2 \nabla\cdot\mathbf{E}, \tag{1}$$

where $H_0$ is the Hamiltonian of the isolated atom and $r$ is the distance between the electron $e_0$ and the atomic nucleus. The second term in (1) describes the plasma ions-emitter dipole interaction, where $\mathbf{d} = -e_0\mathbf{r}$ is the dipole moment and $\mathbf{E} = \{E_i\}$ is the electric microfield strength given by

$$\mathbf{E} = \sum_\alpha \mathbf{E}_\alpha = -\sum_\alpha \frac{q_\alpha \mathbf{R}_\alpha}{R_\alpha^3}(1 + R_\alpha/D)\exp(-R_\alpha/D), \tag{2}$$

where $\alpha$ counts the ions with charges $q_\alpha$ at positions $\mathbf{R}_\alpha = \{X_{\alpha,i}\}$ relative to the atomic nucleus; $D = (k_B T/4\pi e_0 n_e)^{1/2}$ is the electronic Debye radius. The third term in (1) represents the quadrupole interaction of the radiator with inhomogeneous electric microfield of the plasma ions, where $Q_{ij} = -e_0(3x_i x_j - \delta_{ij} r^2)$ is the quadrupole tensor and $E_{ij}$ the inhomogeneous microfield tensor. This symmetrical $E_{ij} = E_{ji}$ and traceless $\mathrm{Tr}\{E_{ij}\} = 0$ tensor has been defined as follows

$$E_{ij} = \partial E_i/\partial x_j - 1/3\,\delta_{ij}\nabla\cdot\mathbf{E}, \tag{3a}$$

and is given by

$$E_{ij} = \sum_\alpha E_{\alpha,ij} = -\sum_\alpha \frac{q_\alpha}{R_\alpha^5}[1 + R_\alpha/D + (R_\alpha/D)^2/3] \cdot \exp(-R_\alpha/D)(3X_{\alpha,i}X_{\alpha,j} - \delta_{ij}R_\alpha^2). \tag{3b}$$

This tensor is used in (1) instead of the field gradients $\partial E_i/\partial x_j$, because the divergence $\nabla\cdot\mathbf{E}$ of the Debye field differs from zero and equals

$$\nabla\cdot\mathbf{E} = -D^{-2}\sum_\alpha q_\alpha/R_\alpha \exp(-R_\alpha/D).$$

Because of (typical $R_\alpha) \approx R_0 \ll D$, then $|\nabla\cdot\mathbf{E}|/|E_{ij}| \approx (R_0/D)^2 = \rho^2 \ll 1$, the last term in (1) is omitted here. ($R_0$ is the distance defined by the relationship (4/15) $(2\pi)^{3/2} R_0^3 n_e = 1$). Therefore the quantities $E_{ij} \cong \partial E_i/\partial x_j$ are approximately equal to the gradients of the ionic field and henceforth they will simply be referred to as the field gradients.

The joint probability density for the microfield strength $\mathbf{E}$ and the microfield gradients $E_{ij}$ (with five independent components in coordinates $xyz$, where generally $\mathbf{E} \nparallel 0z$) is given by [7]

$$W(\mathbf{E}, \mathbf{G}) = \frac{1}{(2\pi)^8}\int \mathrm{d}^3k \int \mathrm{d}^5\sigma \cdot \exp\{-i[\mathbf{k}\cdot\mathbf{E} + \boldsymbol{\sigma}\cdot\mathbf{G}]\} F(\mathbf{k}, \boldsymbol{\sigma}), \tag{4a}$$

where, for convenience, the tensor $E_{ij}$ is represented as a five-dimensional vector

$$\mathbf{G} = \{G_j\} \equiv \{E_{XX}, E_{ZZ}, E_{XY}, E_{XZ}, E_{YZ}\}. \tag{4b}$$

In the case of a plasma containing ions of only one kind (i.e. $q_\alpha = \mathrm{const}$) with density $n$, the Fourier transform has the form

$$F(\mathbf{k}, \boldsymbol{\sigma}) = \exp\left\{\sum_{p=1}^{\infty} \frac{n^p}{p!} h_p(\mathbf{k}, \boldsymbol{\sigma})\right\}. \tag{5}$$

The functions $h_p(\mathbf{k}, \boldsymbol{\sigma})$ correspond to increasing orders in a cluster expansion [18–20]. For small $|\sigma_j|$, the Fourier transform has the series expansion

$$F(\mathbf{k}, \boldsymbol{\sigma}) = F^{(0)}(\mathbf{k}) + \sum_{j=1}^{5} F_j^{(1)}(\mathbf{k})\,\sigma_j, \tag{6a}$$

where

$$F_j^{(1)}(\mathbf{k}) \equiv F^{(0)}(\mathbf{k}) \sum_{p=1}^{\infty} \frac{n^p}{p!} h_{p,j}^{(1)}(\mathbf{k}) \tag{6b}$$

with

$$h_{p,j}^{(1)}(\mathbf{k}) \equiv [\partial h_p(\mathbf{k}, \boldsymbol{\sigma})/\partial\sigma_j]_{\boldsymbol{\sigma}=\mathbf{0}}. \tag{6c}$$

The function $F^{(0)}(\mathbf{k})$ is the Fourier transform of the field distribution function $W(\mathbf{E})$ given by

$$F^{(0)}(\mathbf{k}) = \exp\left\{\sum_{p=1}^{\infty} \frac{n^p}{p!} h_p^{(0)}(\mathbf{k})\right\} \tag{6d}$$

with $h_p^{(0)}(\mathbf{k}) \equiv h_p(\mathbf{k}, \mathbf{0})$.

For calculations of the line profiles, the constrained averages of the field gradients $\langle E_{ij}\rangle_{\mathbf{E}}$ are useful ([7], see also [10, 21]). They are defined by

$$\langle G_j\rangle_{\mathbf{E}} \equiv \int \mathrm{d}^5 G\, G_j W(\mathbf{E}, \mathbf{G})/W(\mathbf{E}) \tag{7}$$

and can be calculated [7, 13] from

$$W(\mathbf{E})\langle G_j\rangle_{\mathbf{E}} = -\frac{i}{8\pi^3}\int \mathrm{d}^3k \exp(-i\mathbf{k}\cdot\mathbf{E}) \cdot [\partial F(\mathbf{k}, \boldsymbol{\sigma})/\partial\sigma_j]_{\boldsymbol{\sigma}=\mathbf{0}}. \tag{8}$$

The present calculation includes only the first two terms of the series in (5) and (6). The derivative of the Fourier

transform can be written

$$[\partial F(\mathbf{k}, \boldsymbol{\sigma})/\partial \sigma_j]_{\boldsymbol{\sigma}=\mathbf{0}} = [n h^{(1)}_{1,j}(\mathbf{k}) + \tfrac{1}{2} n^2 h^{(1)}_{2,j}(\mathbf{k})]\, F^{(0)}(\mathbf{k}) \quad (9\,\mathrm{a})$$

with

$$F^{(0)}(\mathbf{k}) = \exp[n h^{(0)}_1(\mathbf{k}) + \tfrac{1}{2} n^2 h^{(0)}_2(\mathbf{k})]. \quad (9\,\mathrm{b})$$

Introducing the reduced modulus of the field strength $\beta = E/E_0$, the field gradients $\langle E_{ij} \rangle_{\mathbf{E}}$ become

$$\langle E_{ij} \rangle_{\mathbf{E}} = \frac{5}{(32\pi)^{1/2}} \frac{E_0}{R_0} B_\rho(\beta) A_{ij}(\Theta_E, \varphi_E), \quad (10)$$

where the angle functions $A_{ij}(\Theta_E, \varphi_E)$ are given by (A4), angles $\Theta_E$ and $\varphi_E$ being the spherical coordinates of the vector $\mathbf{E}$, and $E_0 = e_0/R_0^2$ is the normal field. As a generalization of the Chandrasekhar and von Neumann function $B(\beta) = B_0(\beta)$, the function $B_\rho(\beta)$ includes ion screening and correlations in the Mozer-Baranger Limit. It

**Table 1.** The generalized function of Chandrasekhar and von Neumann $B_\rho(\beta)$ at a neutral point for singly charged perturbers

| $\beta$ | $B_\rho(\beta)$ | | | | |
|---|---|---|---|---|---|
| | 0.0 | 0.2 | 0.4 | 0.6 | 0.8 |
| 0.10 | 0.1854 E−02 | 0.2860 E−02 | 0.4222 E−02 | 0.6083 E−02 | 0.8702 E−02 |
| 0.20 | 0.7434 E−02 | 0.1147 E−01 | 0.1694 E−01 | 0.2440 E−01 | 0.3479 E−01 |
| 0.30 | 0.1680 E−01 | 0.2594 E−01 | 0.3832 E−01 | 0.5512 E−01 | 0.7822 E−01 |
| 0.40 | 0.3004 E−01 | 0.4644 E−01 | 0.6862 E−01 | 0.9854 E−01 | 0.1390 E+00 |
| 0.50 | 0.4729 E−01 | 0.7319 E−01 | 0.1082 E+00 | 0.1550 E+00 | 0.2171 E+00 |
| 0.60 | 0.6873 E−01 | 0.1065 E+00 | 0.1575 E+00 | 0.2250 E+00 | 0.3127 E+00 |
| 0.70 | 0.9457 E−01 | 0.1468 E+00 | 0.2170 E+00 | 0.3090 E+00 | 0.4258 E+00 |
| 0.80 | 0.1251 E+00 | 0.1944 E+00 | 0.2872 E+00 | 0.4074 E+00 | 0.5565 E+00 |
| 0.90 | 0.1605 E+00 | 0.2498 E+00 | 0.3689 E+00 | 0.5206 E+00 | 0.7048 E+00 |
| 1.00 | 0.2013 E+00 | 0.3136 E+00 | 0.4624 E+00 | 0.6491 E+00 | 0.8709 E+00 |
| 1.10 | 0.2478 E+00 | 0.3864 E+00 | 0.5685 E+00 | 0.7933 E+00 | 0.1055 E+01 |
| 1.20 | 0.3004 E+00 | 0.4687 E+00 | 0.6878 E+00 | 0.9534 E+00 | 0.1256 E+01 |
| 1.30 | 0.3597 E+00 | 0.5612 E+00 | 0.8207 E+00 | 0.1130 E+01 | 0.1474 E+01 |
| 1.40 | 0.4262 E+00 | 0.6646 E+00 | 0.9679 E+00 | 0.1322 E+01 | 0.1710 E+01 |
| 1.50 | 0.5004 E+00 | 0.7796 E+00 | 0.1130 E+01 | 0.1531 E+01 | 0.1962 E+01 |
| 1.60 | 0.5830 E+00 | 0.9067 E+00 | 0.1306 E+01 | 0.1756 E+01 | 0.2232 E+01 |
| 1.70 | 0.6746 E+00 | 0.1047 E+01 | 0.1498 E+01 | 0.1998 E+01 | 0.2517 E+01 |
| 1.80 | 0.7761 E+00 | 0.1200 E+01 | 0.1706 E+01 | 0.2256 E+01 | 0.2819 E+01 |
| 1.90 | 0.8880 E+00 | 0.1368 E+01 | 0.1929 E+01 | 0.2529 E+01 | 0.3136 E+01 |
| 2.00 | 0.1011 E+01 | 0.1550 E+01 | 0.2168 E+01 | 0.2819 E+01 | 0.3469 E+01 |
| 2.10 | 0.1146 E+01 | 0.1746 E+01 | 0.2423 E+01 | 0.3125 E+01 | 0.3816 E+01 |
| 2.20 | 0.1294 E+01 | 0.1959 E+01 | 0.2694 E+01 | 0.3445 E+01 | 0.4179 E+01 |
| 2.30 | 0.1456 E+01 | 0.2187 E+01 | 0.2980 E+01 | 0.3781 E+01 | 0.4555 E+01 |
| 2.40 | 0.1632 E+01 | 0.2430 E+01 | 0.3282 E+01 | 0.4131 E+01 | 0.4945 E+01 |
| 2.50 | 0.1822 E+01 | 0.2690 E+01 | 0.3599 E+01 | 0.4496 E+01 | 0.5349 E+01 |
| 2.60 | 0.2029 E+01 | 0.2966 E+01 | 0.3931 E+01 | 0.4874 E+01 | 0.5767 E+01 |
| 2.70 | 0.2251 E+01 | 0.3258 E+01 | 0.4278 E+01 | 0.5266 E+01 | 0.6198 E+01 |
| 2.80 | 0.2490 E+01 | 0.3566 E+01 | 0.4640 E+01 | 0.5670 E+01 | 0.6642 E+01 |
| 2.90 | 0.2746 E+01 | 0.3890 E+01 | 0.5016 E+01 | 0.6088 E+01 | 0.7099 E+01 |
| 3.00 | 0.3020 E+01 | 0.4229 E+01 | 0.5406 E+01 | 0.6518 E+01 | 0.7568 E+01 |
| 3.20 | 0.3620 E+01 | 0.4954 E+01 | 0.6227 E+01 | 0.7413 E+01 | 0.8535 E+01 |
| 3.40 | 0.4290 E+01 | 0.5739 E+01 | 0.7101 E+01 | 0.8354 E+01 | 0.9548 E+01 |
| 3.60 | 0.5030 E+01 | 0.6581 E+01 | 0.8025 E+01 | 0.9340 E+01 | 0.1062 E+02 |
| 3.80 | 0.5838 E+01 | 0.7480 E+01 | 0.8996 E+01 | 0.1038 E+02 | 0.1172 E+02 |
| 4.00 | 0.6711 E+01 | 0.8435 E+01 | 0.1001 E+02 | 0.1147 E+02 | 0.1284 E+02 |
| 4.25 | 0.7889 E+01 | 0.9694 E+01 | 0.1135 E+02 | 0.1288 E+02 | 0.1431 E+02 |
| 4.50 | 0.9156 E+01 | 0.1102 E+02 | 0.1274 E+02 | 0.1435 E+02 | 0.1584 E+02 |
| 4.75 | 0.1051 E+02 | 0.1243 E+02 | 0.1420 E+02 | 0.1586 E+02 | 0.1742 E+02 |
| 5.00 | 0.1193 E+02 | 0.1389 E+02 | 0.1571 E+02 | 0.1742 E+02 | 0.1905 E+02 |
| 5.50 | 0.1499 E+02 | 0.1699 E+02 | 0.1890 E+02 | 0.2072 E+02 | 0.2244 E+02 |
| 6.00 | 0.1829 E+02 | 0.2032 E+02 | 0.2231 E+02 | 0.2422 E+02 | 0.2603 E+02 |
| 6.50 | 0.2180 E+02 | 0.2384 E+02 | 0.2588 E+02 | 0.2789 E+02 | 0.2974 E+02 |
| 7.00 | 0.2551 E+02 | 0.2754 E+02 | 0.2965 E+02 | 0.3167 E+02 | 0.3373 E+02 |
| 8.00 | 0.3344 E+02 | 0.3546 E+02 | 0.3764 E+02 | 0.3988 E+02 | 0.4210 E+02 |
| 9.00 | 0.4199 E+02 | 0.4400 E+02 | 0.4621 E+02 | 0.4851 E+02 | 0.5079 E+02 |
| 10.00 | 0.5110 E+02 | 0.5308 E+02 | 0.5537 E+02 | 0.5785 E+02 | 0.6025 E+02 |
| 12.00 | 0.7082 E+02 | 0.7264 E+02 | 0.7521 E+02 | 0.7790 E+02 | 0.8089 E+02 |
| 14.00 | 0.9235 E+02 | 0.9407 E+02 | 0.9675 E+02 | 0.9972 E+02 | 0.1030 E+03 |
| 16.00 | 0.1156 E+03 | 0.1174 E+03 | 0.1200 E+03 | 0.1230 E+03 | 0.1261 E+03 |
| 18.00 | 0.1403 E+03 | 0.1422 E+03 | 0.1448 E+03 | 0.1480 E+03 | 0.1513 E+03 |
| 20.00 | 0.1664 E+03 | 0.1683 E+03 | 0.1710 E+03 | 0.1743 E+03 | 0.1780 E+03 |

can be expressed by auxiliary functions $\Psi(v)$, which are calculated in Appendix A:

$$B_\rho(\beta)=\frac{2}{\pi}\beta^2/W_\rho(\beta)\int_0^\infty \mathrm{d}x\,x^2[\Psi_1^{(1)}(v)+\Psi_2^{(1)}(v)]\cdot\exp\{-x^{3/2}[\Psi_1^{(0)}(v)-\Psi_2^{(0)}(v)]\}j_2(\beta x), \tag{11}$$

with the static ion microfield probability density in the Mozer-Baranger limit [19, 20]

$$W_\rho(\beta)=4\pi E_0^3\beta^2 W(\mathbf{E})=\frac{2}{\pi}\beta^2\int_0^\infty \mathrm{d}x\,x^2\exp\{-x^{3/2}[\Psi_1^{(0)}(v)-\Psi_2^{(0)}(v)]\}j_0(\beta x). \tag{12}$$

(Our recalculated values of $W_\rho(\beta)$ are in very good agreement with those in paper [20]. This agreement confirms the numerical code used in our calculations.)

For the present study, the function $B_\rho(\beta)$ has been calculated at a neutral point in a singly ionized ($q_z=e_0$) isothermal ($T_{\mathrm{ion}}=T_{\mathrm{el}}=T$) plasma. Values of $B_\rho(\beta)$ are given in Table 1. At $\rho=0$, this function reduces to the ordinary Chandrasekhar and von Neumann function [13], tabulated by Demura and Sholin [7]. Taking into account screening and correlation effects leads to considerable increase of $B_\rho(\beta)$ as compared with $B(\beta)$. As can be seen in Fig. 1, the discrepancy between $B_\rho(\beta)$ and $B(\beta)$ increases with increasing parameter $\rho$. This is a measure of the importance of the effects included in the present calculations.

To describe the contribution of the atom-ion quadrupole interaction to the H-line profile, the authors of [7] introduced two further universal functions $\Lambda(\beta)$ and $\chi(\beta)$. As a result of the generalization in the Mozer-Baranger Limit, the corresponding functions $\Lambda_\rho(\beta)$ and $\chi_\rho(\beta)$, defined by Demura and Sholin [7], become

$$\Lambda_\rho(\beta)=W_\rho(\beta)\cdot B_\rho(\beta)/\beta$$

and

$$\chi_\rho(\beta)=-\frac{\mathrm{d}}{\mathrm{d}\beta}[W_\rho(\beta)\cdot B_\rho(\beta)].$$

These functions are presented in Figs. 2 and 3. The conclusions concerning these functions are analogous to those concerning $B_\rho(\beta)$.

## 3. The H-line profiles

In the static ion approximation including the quadrupole interaction of the emitter with the electric microfield gradients of the perturbing ions, the line shape function is given by [7]

$$P(\omega)=\int \mathrm{d}^3E\int \mathrm{d}G^5\,W(\mathbf{E},\mathbf{G})\,P(\omega,\mathbf{E},\mathbf{G}), \tag{13}$$

where $P(\omega,\mathbf{E},\mathbf{G})$ is the electron-broadend line profile for a given field $\mathbf{E}$ and field gradients $\mathbf{G}$ (see (4b)). The electron-broadened line profile for a radiator transition

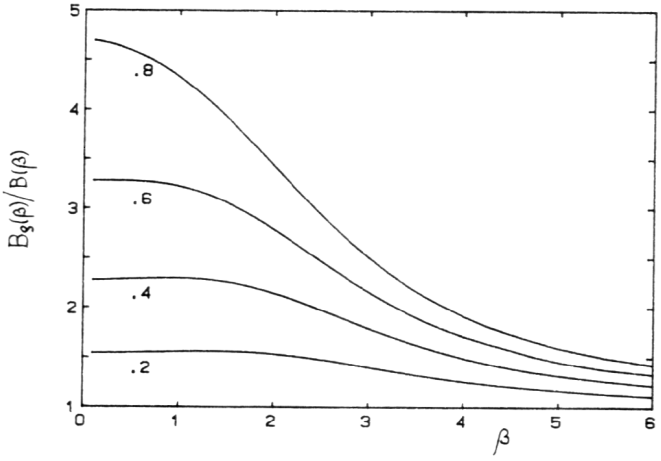


**Fig. 1.** Ratio of the generalized Chandrasekhar and von Neumann $B_\rho(\beta)$ function and the ordinary function $B(\beta)$ (i.e. $B_\rho(\beta)$ at $\rho=0$) as a function of the reduced field strength $\beta$, for several values of $\rho=R_0/D$

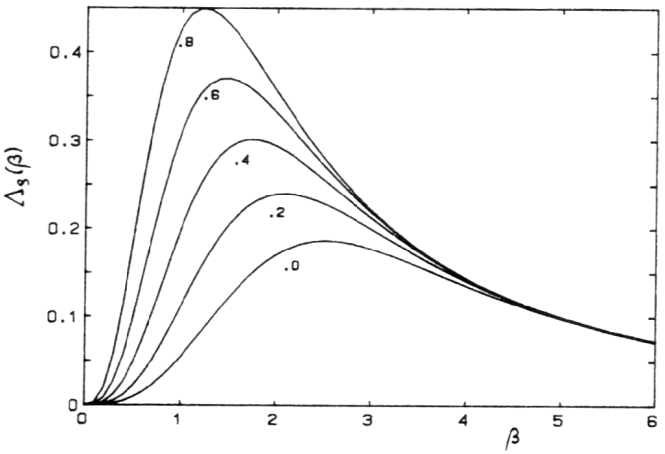


**Fig. 2.** $\Lambda_\rho(\beta)$ as a function of the reduced field $\beta$, for several $\rho$ values

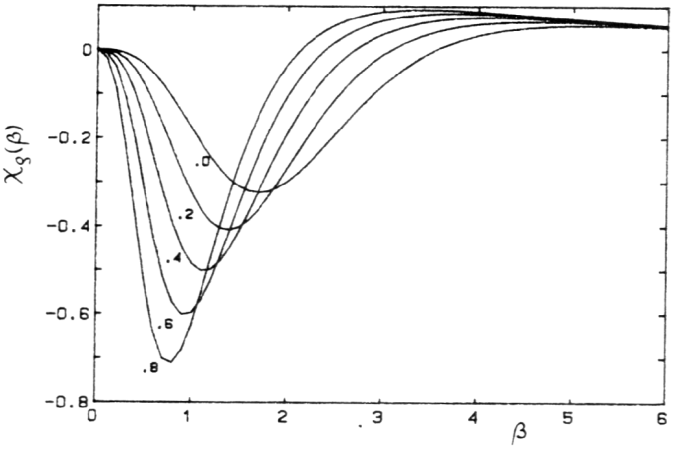


**Fig. 3.** $\chi_\rho(\beta)$ as a function of the reduced field $\beta$, for several $\rho$ values

from an initial state $n$ to a final state $n'$ can be described by [1]

$$P(\omega, \mathbf{E}, \mathbf{G}) = \frac{1}{\pi} \operatorname{Re} \sum_{aba'b'} \langle a|\mathbf{d}|a'\rangle\langle b'|\mathbf{d}|b\rangle \cdot\langle a|\langle a'|[i\omega - i(H_n - H_{n'})] - \Phi_{nn'}]^{-1}|b\rangle|b'\rangle, \quad (14)$$

where $\Phi_{nn}$, is the operator of impact electron broadening for the $n \to n'$ transition, and $ab$ and $a'b'$ numerate the Stark sublevels of the initial and final state, respectively.

In order to proceed with the calculation, we introduce (similarly as in [7, 10, 21]) the simplifying approximation

$$\int d^5 G\, W(\mathbf{E}, \mathbf{G})\, P(\omega, \mathbf{E}, \mathbf{G}) = W(\mathbf{E})\, P(\omega, \mathbf{E}, \langle \mathbf{G}\rangle_{\mathbf{E}}), \quad (15)$$

which is exact to linear order in $\langle \mathbf{G}\rangle_{\mathbf{E}}$ [10]. Making use of the tracelessness and the symmetry of tensors $E_{ij}$ and $Q_{ij}$, in the coordinate system $xyz$ with $\mathbf{E} \| 0z$, the term describing the emitter-ion quadrupole interaction $H_q$ in the Hamiltonian (1) can be expressed in terms of the mean field gradients

$$H_q = -\tfrac{1}{6}[2Q_{xx} + Q_{zz})\langle E_{xx}\rangle_{\mathbf{E}} + (2Q_{zz} + Q_{xx})\langle E_{zz}\rangle_{\mathbf{E}} + 2Q_{xy}\langle E_{xy}\rangle_{\mathbf{E}} + 2Q_{xz}\langle E_{xz}\rangle_{\mathbf{E}} + 2Q_{yz}\langle E_{yz}\rangle_{\mathbf{E}}]. \quad (16)$$

Taking into account the axial symmetry of $\langle E_{ij}\rangle_{\mathbf{E}}$ with respect to the field vector $\mathbf{E}$ (see (A4)), after passing to the coordinate system $x'y'z'$ with $\mathbf{E} \| 0z'$ the operator $H_q$ is proportional to the $Q_{z'z'}$ tensor component. Thus, in this approximation the Hamiltonian in (14), in the dimensionless field scale, is given by

$$H = H_0 + e_0 E_0 \beta z' - \frac{5}{(32\pi)^{1/2}} \frac{e_0 E_0}{2R_0} B_p(\beta)(3z'^2 - r'^2), \quad (17)$$

whereby the line shape function (13) reduces to the ordinary form [1]

$$P(\omega) = \int_0^\infty d\beta\, W_p(\beta)\, P(\omega, \beta). \quad (18)$$

Calculations of $P(\omega)$ haved been performed exact to terms of the order of $(a_0/R_0)^4$ ($a_0$ – the Bohr radius), i.e. the dipole terms, the multi-ion-emitter-quadrupole interaction and the quadratic Stark effect have been taken into account. The matrix elements in (14) of the operators $\mathbf{d}$, $H$, and $\Phi_{nn'}$ for the dipole terms have been taken as in [1], for the quadrupole terms (for replacing $B_0(\beta)$ by $B_p(\beta)$) as in [7, see also 6 and 9] and for the quadratic Stark effect as in [9]. In the frame of this accuracy, it is sufficient to use only the off-diagonal dipole matrix elements for the operator $\Phi_{nn'}$. For the numerical calculations the values of $W_p(\beta)$ have been taken from [17].

As is well known, the relationship between the line profile $P(\Delta\omega)$ and the line intensity $I(\Delta\omega)$ are related by

$$I(\Delta\omega) = I(\omega_0)(1 + \Delta\omega/\omega_0)^4 \exp(-\hbar\Delta\omega/k_B T)\, P(\Delta\omega), \quad (19)$$

where $\omega_0$ is the angular frequency of the unperturbed line, and $\Delta\omega$ denotes the frequency distance, $\Delta\omega = \omega - \omega_0$. The factor in front of $P(\Delta\omega)$ contributes an additional asymmetry, the so-called trivial asymmetry, which has to be taken into account in comparisons with measured line asymmetries.

## 4. Comparison with measurements of $H_\beta$ line and conclusions

The $H_\beta$ line has three characteristic points: the blue and red peaks and the central dip. According to the formalism described above, the intensities $I$ and the wavelengths $\lambda$ of these points and the asymmetry parameters

$$\delta I = (I_B - I_R)/I_{B'} \quad (20a)$$

$$\delta\lambda_{P-D} = (\lambda_B + \lambda_R)/2 - \lambda_D \quad (20b)$$

have been calculated. The calculated values are compared with numerous measurements [9, 22–30] in Figs. 4 and 5, which show that agreement between theory and

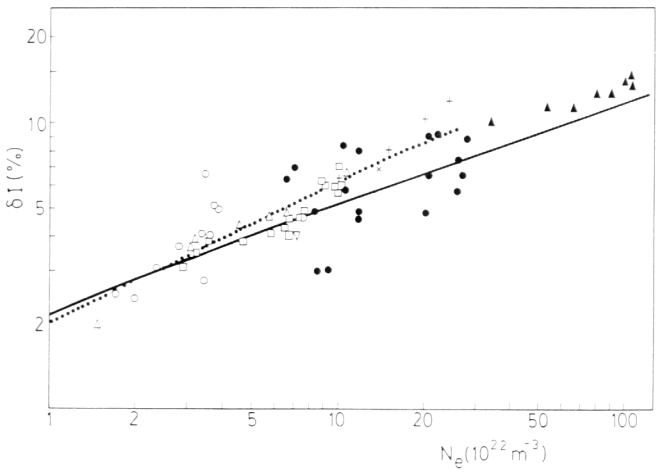


**Fig. 4.** Comparison of the measured asymmetry of the $H_\beta$ peaks (data points) with the result of present calculations (solid line). The measured values are taken from [9] (□), [22] (▽), [23] (■), [24] (+), [25] (×), [26] (...), [27] (△), [28] (○), [29] (▲), [30] (●)

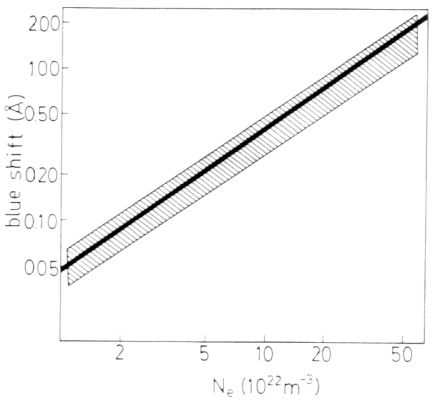


**Fig. 5.** Comparison of the measured (shaded area [12]) shifts $\delta\lambda_{P-D}$ of the $H_\beta$ peaks with the present calculations (solid line)

measurements is good. This was an encouragement for calculating the whole profile $P(\Delta\omega)$. However, due to the long duration of such numerical calculations, detailed computations have been carried out only for one case: $n_e = 10^{17}\,\mathrm{cm}^{-3}$ and $T = 13000\,\mathrm{K}$. These values of $n_e$ and $T$ were selected to compare the theory with the theoretical data from [4]. From the experimental data of earlier work [9] (hydrogen-argon arc-plasma), the $H_\beta$ line profile averaged over 6 measurements and corresponding to the physical conditions nearest to those above, i.e. $n_e = 9.9 \times 10^{16}\,\mathrm{cm}^{-3}$ and $T = 12900\,\mathrm{K}$, was selected for comparison with the calculations. Because hydrogen line profiles in the scale $\alpha = \Delta\lambda/E_0$ depend very weakly on $n_e$ and $T$(cf. [1]), the theoretical profile was reduced to the experimental conditions using the proper values of $E_0$. The quantity $\Delta\lambda$ is $\Delta\lambda \equiv -\Delta\omega\lambda_0^2/(2\pi c)$ with $\lambda_0$ as the wavelength of the unperturbed line. The scale $\Delta\lambda$ is proportional to $\Delta\omega$ and does not cause any "artificial" asymmetry of the profile in a result of the transition from $\omega$ to $\lambda$.

In the present study the shift $\Delta\lambda_{el}$, resulting from interactions of the emitter with free electrons, has been omitted in $P(\Delta\omega)$. However, as discussed in paper [12], the assumption $\Delta\lambda_{el} = \text{const.}$ seems to be well satisfied in the whole line profile. Thus, in order to compare the calculated line profile with the experimental one, the theoretical profile should be shifted by $\Delta\lambda_{el}$ (or the measured profil should be shifted by $-\Delta\lambda_{el}$). Figure 6 shows the best fit of the experimental and theoretical profiles with $\Delta\lambda_{el}$ as the free parameter of the fitting procedure. In the case examined we obtained $\Delta\lambda_{el} = 1.30$ Å. The reason of the discrepancy in the central part of the profile is the omission of ion dynamic effects in the calculations. In order to free of our analysis concerning the asymmetry from these effects, the differences $\Delta P$ between blue and red profile wings $\Delta P = P_B(-\Delta\lambda') - P_R(\Delta\lambda')$, are compared for theoretical and measured data in Fig. 7. For that analysis the scale $\Delta\lambda' = \Delta\lambda - \Delta\lambda_{el}$ is used. As seen in Fig. 7, a good agreement was achieved, except around the maximum of $\Delta P$, i.e. in the region of the half width of the line profile. (In that region the efficiency of the ion-quadrupole interaction is greatest.) The observed discrepancy can result from uncertainties of the measurements and from a corresponding uncertainty of the $\Delta\lambda_{el}$ value. Generally, however, the analysis shows that the formalism presented in this paper describes the asymmetry $H_\beta$ produced by ion interactions rather well. For a decisive rating, further comparisons with measurements are needed also for other H-lines.

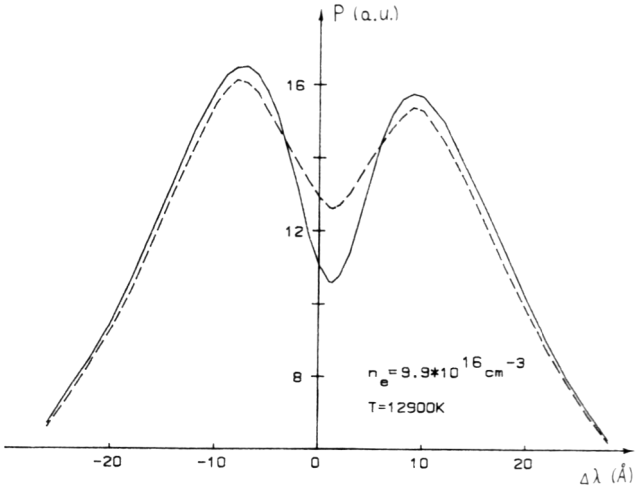


**Fig. 6.** Comparison of the central part of the measured (dashed line [9]) $H_\beta$ line profile with the present calculations (solid line) vs. the wavelength distance $\Delta\lambda$ from the unperturbed wavelength $\lambda_0$. The red shift is $\Delta\lambda_{el} = 1.30$ Å

The quantity $\Delta\lambda_{el}$ has been evaluated also in other selected regions of the $H_\beta$ line on the basis of the relationship $\Delta\lambda_{el} = \Delta\lambda_{\text{total}}^{\text{expt}} - \Delta\lambda_{\text{ion}}^{\text{th}}$. The obtained results are gathered in Table 2. The symbols used have the following meaning: the experimental line center (ELC) is defined [31] as the arithmetic mean of the shift at 1/2, 1/4, and 1/8 of the average height $P_{\text{av}} = (P_B + P_R)/2$, whereas the dip shift is defined [11] by $\delta\lambda = \lambda_D - \lambda_0$, and the peaks shift by (20b). In all cases the obtained values $\Delta\lambda_{el}$ are practically the same, which confirms the assumption that $\Delta\lambda_{el} \cong \text{const.}$ in the whole line profile. There are, however, about 30 percent discrepancy with the theoretical predictions of the numerical value of this quantity. It should be noted, furthermore, that the ion contribution to the ELC shift is about threefold greater than recommended theoretically [3, 4]. Therefore it seems to be appropriate to re-evaluate also ion-produced blue shifts,

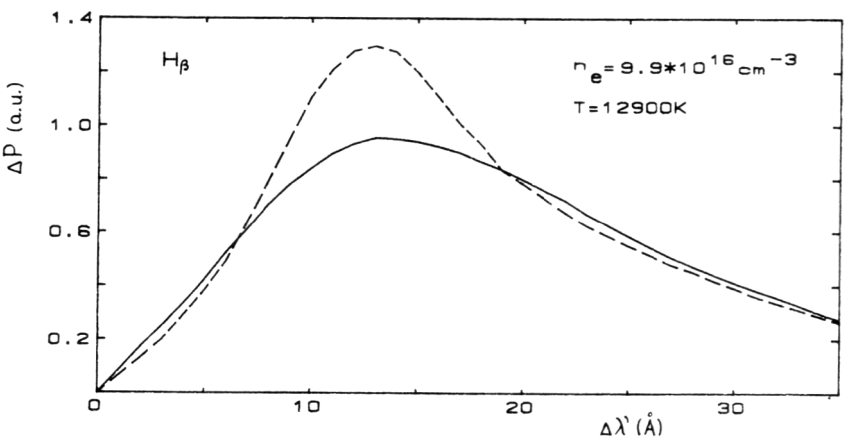


**Fig. 7.** Comparison of the measured difference $\Delta P$ between blue and red profile wings (dashed line) with the present calculations (solid line), vs. relative wavelength $\Delta\lambda'$

**Table 2.** Comparison of measured and calculated wavelength shifts of $H_\beta$ for different parts of the line profile at a nominal electron density of $10^{17}\,cm^{-3}$. The measured total shift $\Delta\lambda_{total}^{expt}$ is the sum of the ionic shift $\Delta\lambda_{ion}$ and of the electronic shift $\Delta\lambda_{el}$

| Shift (Å) | | | | | |
|---|---|---|---|---|---|
| | $\delta\lambda_{total}^{expt}$ | Ref | $\delta\lambda_{ion}^{th}$ | $\delta\lambda_{el}$ | Ref |
| ELC | 0.70 | 31 | −0.71 | 1.41 | |
| | 0.82 | 32 | | 1.53 | |
| dip | 1.50 | 11 | 0.07 | 1.43 | |
| | 1.33 | 12 | | 1.26 | |
| peaks | 0.95 | 12 | −0.42 | 1.37 | |
| total profile fiting | | | | 1.31 | |
| average | | | | 1.385 | |
| theoretical | | | | 1.025 | 4 |
| | | | | 1.759 | 8 |

e.g. in the line profiles of singly ionized helium [33]. This will be the subject of a forthcoming paper.

The author thanks Prof. B. Grabowski for helpful discussions. This work was performed under the partial sponsorship of the Polish Academy of Science and of the scientific program CPBP.01.10.

## Appendix A

The Fourier transform $F(\mathbf{k}, \boldsymbol{\sigma})$ given by (5) is expressed by the functions $h_p(\mathbf{k}, \boldsymbol{\sigma})$ resulting from application of the cluster expansion method [19, 20]. The general expression for a function of $p$-th order is

$$h_p(\mathbf{k}, \boldsymbol{\sigma}) = \int \varphi_1 \varphi_2 \ldots \varphi_p g_p(\mathbf{R}_1, \mathbf{R}_2, \ldots, \mathbf{R}_p) \cdot d^3R_1\, d^3R_2 \ldots d^3R_p \quad (A.1a)$$

with

$$\varphi_\alpha = \exp[i(\mathbf{k}\cdot\mathbf{E}_\alpha + \boldsymbol{\sigma}\cdot\mathbf{G}_\alpha)] - 1, \quad (A.1b)$$

where $g_p$ is the $p$-body correlation function depending on the configuration of $p$ ions located at $\mathbf{R}_1, \mathbf{R}_2, \ldots, \mathbf{R}_p$. The functions $h(\mathbf{k})$ resulting from (A.1) and (6) can be written as follows:

– one-body functions

$$h_1^{(0)} = \int g_1(\mathbf{R}_1)[\exp(i\mathbf{k}\cdot\mathbf{E}_1) - 1]\, d^3R_1 \quad (A.2a)$$

and

$$h_{1,j}^{(1)} = i\int g_1(\mathbf{R}_1)\, G_{1,j} \exp(i\mathbf{k}\cdot\mathbf{E}_1)\, d^3R_1; \quad (A.2b)$$

– two-body functions

$$h_2^{(0)} = \int g_2(\mathbf{R}_1, \mathbf{R}_2)[\exp(i\mathbf{k}\cdot\mathbf{E}_1) - 1] \cdot [\exp(i\mathbf{k}\cdot\mathbf{E}_2) - 1]\, d^3R_1\, d^3R_2 \quad (A.3a)$$

and

$$h_{2,j}^{(1)} = i\int g_2(\mathbf{R}_1, \mathbf{R}_2)\{G_{1,j}\exp(i\mathbf{k}\cdot\mathbf{E}_1)[\exp(i\mathbf{k}\cdot\mathbf{E}_2) - 1] + G_{2,j}\exp(i\mathbf{k}\cdot\mathbf{E}_2)[\exp(i\mathbf{k}\cdot\mathbf{E}_1) - 1]\}\, d^3R_1\, d^3R_2. \quad (A.3b)$$

Here, $\mathbf{E}_\alpha$ and $G_{\alpha,j}$ are the field and field gradient corresponding to a single ion at $\mathbf{R}_\alpha$. In spherical coordinates $R, \Theta_R, \varphi_R$, one can write these quantities as follows:

$$\mathbf{E}_\alpha = -E(R_\alpha)\,\mathbf{R}_\alpha/R_\alpha, \quad (A.4a)$$

$$G_{\alpha,j} = -G(R_\alpha)\, A_j(\Theta_R, \varphi_R), \quad (A.4b)$$

where $E(R_\alpha)$ and $G(R_\alpha)$ are the radial contributions to the field and to the field gradients as described by (2) and (3b), whereas the five independent components of the gradients depend on the angles as follows:

$$A_{xx} = \tfrac{1}{2}P_2^{(2)}(\mu_R)\cos 2\varphi_R - P_2(\mu_R);$$
$$A_{xy} = \tfrac{1}{2}P_2^{(2)}(\mu_R)\sin 2\varphi_R;$$
$$A_{xz} = -P_2^{(1)}(\mu_R)\cos\varphi_R; \qquad A_{yz} = -P_2^{(1)}(\mu_R)\sin\varphi_R;$$
$$A_{zz} = 2P_2(\mu_R)). \quad (A.4c)$$

$P_l^{(m)}(\mu)$ is the Associated Legendre Function, $P_l(\mu)$ the Legendre function, and $\mu_R \equiv \cos\Theta_R$. The functions $h_1^{(0)}$ and $h_2^{(0)}$ given by (A.2a) and (A.3a) have been recalculated applying spherical harmonics development as in papers [19, 20], using the same correlation functions $g_1$ and $g_2$. In a neutral point (for a H-atom) we have

$$g_1 = 1$$

and

$$g_2 = -(4\pi D^2 n_e)^{-1}\,|\mathbf{R}_1 - \mathbf{R}_2|^{-1}\exp(-\sqrt{2}|\mathbf{R}_1 - \mathbf{R}_2|/D).$$

An analogous calculational technique has been used for $h_{1,j}^{(1)}$ and $h_{2,j}^{(1)}$, starting from (A.2b) and (A.3b). Then, the contributions of one-body and two-body clusters in (9), using the auxiliary functions $\Psi(v)$, are:

$$n h_1^{(1)} = -x^{3/2}\,\Psi_1^{(0)}(v),$$
$$\tfrac{1}{2}n^2 h_2^{(0)} = x^{3/2}\,\Psi_2^{(0)}(v),$$
$$n h_{1,j}^{(1)} = -i\,\frac{5}{(32\pi)^{1/2}}\,\frac{E_0}{R_0}\,\Psi_1^{(1)}(v)\,A_j(\Theta_k, \varphi_k),$$
$$\tfrac{1}{2}n^2 h_{2,j}^{(1)} = -i\,\frac{5}{(32\pi)^{1/2}}\,\frac{E_0}{R_0}\,\Psi_2^{(1)}(v)\,A_j(\Theta_k, \varphi_k), \quad (A.5)$$

where the angles $\Theta_k$ and $\varphi_k$ define the direction of $\mathbf{k}$ vector in the coordinate system $xyz$.

For an isothermal singly ionized plasma ($n = n_e$), the functions $\Psi_1^{(0)}$ and $\Psi_2^{(0)}$ are the same as in papers [19, 20]. For the functions $\Psi_1^{(1)}$ and $\Psi_2^{(0)}$ we have derived the expressions

$$\Psi_1^{(1)} = 6\int_0^\infty y_1^2\,\gamma(v, y_1)\,j_2(\varepsilon_1)\,dy_1, \quad (A.6a)$$

$$\Psi_2^{(1)} = 12\sqrt{2}\,v^3 \int_{y_1=0}^{\infty} y_1^2\,dy_1 \int_{y_2=0}^{y_1} y_2^2\,dy_2\,\gamma(v, y_1) \cdot \left[j_2(\varepsilon_1) - \sum_{l=0}^{\infty}(-1)^l(2l+1)\{\tfrac{3}{2}[l(l-1)\varepsilon_1^{-2} - 1]\,j_l(\varepsilon_1) + 3\varepsilon_1^{-1}\,j_{l+1}(\varepsilon_1)\}\,j_l(\varepsilon_2)\right] f_l{>}(u_1)\,f_l{<}(u_2), \quad (A.6b)$$

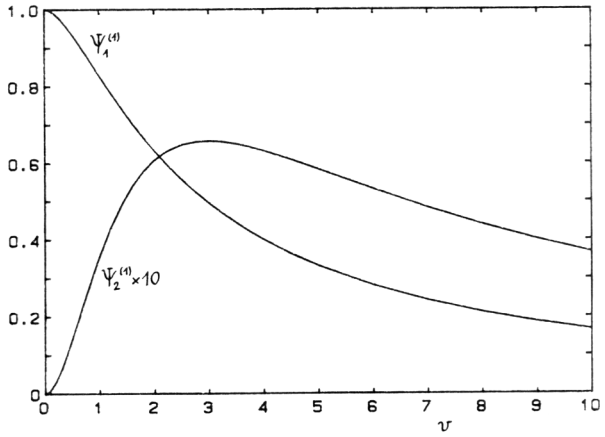


**Fig. 8.** The one-body function $\Psi_1^{(1)}$ and the two-body function $\Psi_2^{(1)}$ at a neutral point for the case of singly charged perturbers vs. the quantity $v$

where $j_l(\varepsilon)$ is the Spherical Bessel Function of order $l$, and $f_l>(u)$ and $f_l<(u)$, defined according to [20], are given by

$$f_l>(u)=(-1)^l u^l\left(\frac{\mathrm{d}}{u\,\mathrm{d}u}\right)^l\left(\frac{e^{-u}}{u}\right)$$

and

$$f_l<(u)=i^{-l}j_l(iu)=u^l\left(\frac{\mathrm{d}}{u\,\mathrm{d}u}\right)^l\left(\frac{\sinh u}{u}\right).$$

The new variables used in (A.6) are defined as follows:

$$v=x^{1/2}\rho \quad \text{with} \quad x=kE_0 \quad (k=|\mathbf{k}|),$$

and

$$\varepsilon(v,y)=kE(R)=y^{-2}(1+vy)\exp(-vy),$$
$$\gamma(v,y)=e_0^{-1}(vD)^3G(R)$$
$$=y^{-3}[1+vy+(vy)^2/3]\exp(-vy),$$

with

$$y=(ke_0)^{-1/2}R$$

and

$$u=\sqrt{2}vy.$$

The functions $\Psi(v)$ have been calculated numerically in the whole variability region of $v$, in contrast to [20], where the asymptotic approximation at $v\approx 0$ was used. The recalculated results for the functions $\Psi_1^{(0)}$ and $\Psi_2^{(0)}$ obtained here are in good agreement with the graphical ones from [20]. The functions $\Psi_1^{(1)}$ and $\Psi_2^{(1)}$ are shown in Fig. 8. At $v=0$ these functions reduce to Holtsmark's approximation, attaining the values $\Psi_1^{(1)}=1$ and $\Psi_2^{(1)}=0$.

## References


1. Kepple, P., Griem, R.: Phys. Rev. **173**, 317 (1968); Griem, H.R.: Spectral line broadening by plasmas. New York: Academic Press 1974
2. Oza, D.H., Green, R.L., Kelleher, D.E.: Phys. Rev. A **37**, 531 (1988)
3. Griem, H.R.: Phys. Rev. A **28**, 1596 (1983)
4. Griem, H.R.: Phys. Rev. A **32**, 2943 (1988)
5. Kudrin, L.P., Sholin, G.V.: Sov. Phys. Dokl. **7**, 1015 (1963)
6. Sholin, G.V.: Opt. Spektrosk. (USSR) **26**, 489 (1969)
7. Demura, A.V., Sholin, G.V.: JQSRT **15**, 881 (1975)
8. Grabowski, B., Halenka, J.: Astron. Astrophys. **45**, 159 (1975)
9. Halenka, J.: JQSRT **39**, 347 (1988)
10. Joyce, R.F., Woltz, L.A., Hooper, C.F., Jr.: Phys. Rev. A **35**, 2228 (1987)
11. Halenka, J., Musielok, J.: JQSRT **36**, 233 (1986)
12. Halenka, J., Vujičić, B., Djurović, S.: JQSRT **42**, 571 (1989)
13. Chandrasekhar, S., von Neumann: Astrophys. J. **97**, 1 (1943)
14. Iglesias, C.A., Hooper, C.F., Jr., DeWitt, H.E.: Phys. Rev. A **28**, 361 (1983)
15. Lewis, M., Margenau, H.: Phys. Rev. **109**, 842 (1958); Rev. Mod. Phys. **31**, 569 (1959)
16. Ecker, G.: Z. Phys. **148**, 593 (1957); Ecker, G., Müller, K.G.: Z. Phys. **153**, 317 (1958)
17. Hooper, C.F., Jr.: Phys. Rev. **165**, 215 (1968)
18. Mayer, J.E., Mayer, M.G.: Statistical mechanics of fluids. New York: Kiley 1940
19. Baranger, M., Mozer, B.: Phys. Rev. **115**, 521 (1959); Mozer, B., Baranger, M.: Phys. Rev. **118**, 626 (1960)
20. Pfennig, H., Trefftz, E.: Z. Naturforsch. **21a**, 697 (1966)
21. Gaisinsky, I.M., Oks, E.A.: JQSRT **41**, 235 (1989)
22. Wende, B.: Z. Angew. Phys. **22**, 181 (1966)
23. Wiese, W.L., Kelleher, D.E.: Proceedings of the 10th ICPIG, p. 377, Oxford (1971)
24. Okasaka, R., Nagashima, M., Fukuda, K.: J. Phys. Soc. Japan **42**, 1339 (1977)
25. Preston, R.C.: JQSRT **18**, 337 (1977)
26. Chotin, J.L., Lemaire, J.L., Marque, J.P., Rostas, F.: J. Phys. B: At. Molec. Phys. **14**, 3573 (1981)
27. Helbig, V., Nick, K.P.: J. Phys. B: At. Mol. Phys. **14**, 3573 (1981)
28. Torres, F., Gigosos, M.A., Mar, S.: JQSRT **31**, 265 (1984)
29. Carlhoff, C., Krametz, E., Schafer, J.H., Uhlenbusch, J.: J. Phys. B: Atom. Molec. Phys. **19**, 2629 (1986)
30. Mijatović, Z., Pavlov, M., Djurović, S.: JQSRT **38**, 209 (1987)
31. Wiese, W.L., Kelleher, D.E., Paquette, D.R.: Phys. Rev. A **26**, 1132 (1972)
32. Pitman, T.L., Kelleher, D.E.: In: Spectral line shapes. Wende, B. (ed.), p. 165. Berlin: DeGruytz 1981
33. Griem, H.R.: Phys. Rev. A **27**, 2566 (1983)